Electrochemical-driven water reduction and oxidation catalyzed by an iron(III) complex supported by 2,3-bis(2-hydroxybenzylideneimino)-2,3-butenedinitrile

Ling-Zhi Fu, Ling-Ling Zhou, Shu-Zhong Zhan*

College of Chemistry and Chemical Engineering, South China University of Technology, Guangzhou 510640, China

Supplementary Materials

Table of context

7	**Fig. S7**. CV of ligand (3.17 mM) and $FeCl_3$ (3.17 mM) (1:1) in 0.1 M of [n-Bu_4N]ClO_4 DMF solution. GC working electrode (1 mm diameter), Pt counter electrode, Ag/$AgNO_3$ reference electrode, scan rate 100 mV/s.
8	**Fig. S8.** Turnover frequency (mol H_2/mol catalysts/h) for electrocatalystic hydrogen production by complex **1** (5.80 μM) under overpotentials.
9	**Fig. S9.** Cyclic voltammograms of complex **1** (1.71 mM) in different pHs. Conditions: 0.25 M phosphate buffered solutions (KH_2PO_4 + NaOH), GC working electrode (1.0 mm diameter), Pt wire counter electrode, Ag/AgCl reference electrode.
10	**Fig. S10.** Cyclic voltammogram of complex **1** (1.05 mM) in different scan rate. Conditions: 0.25 M phosphate buffered solution (pH 7.0), GC working electrode (1.0 mm diameter), Pt wire counter electrode, Ag/AgCl reference electrode.
11	**Fig. S11.** Bubbles form
12	**Fig. S12**. (a) GC traces after a 1h controlled-potential electrolysis at −1.45 V *vs* Ag/AgCl of 17.4 μM complex **1** in 0.25 M buffer, pH 7.0. A standard of CH_4 was added for calibration purposes. (b) Measured (red) and calculated (black) pH changes assuming a 100% Faradic efficiency of complex **1** during electrolysis. (the theoretical pH change over time can be calculated by the equation of $pH = 14 + \lg\frac{\sum It}{FV}$ where I = current (A), t = time (s), F = Faraday constant (96485 C/mol), V = solution volume (0.04 L)).
13	**Fig. S13.** (a) Scan rate dependence of precatalytic waves for $Fe^{IV/III}$ and $Fe^{V/IV}$ couples from a 1.71 mM solution of complex **1** in buffer (pH 10.5), at scan rates from 50 to 200 mV/s. (b) Linear fitting plot of i_{cat} *vs* $v^{-1/2}$ for $Fe^{IV/III}$. (c) Linear fitting plot of i_{cat} *vs* $v^{-1/2}$ for $Fe^{V/IV}$.

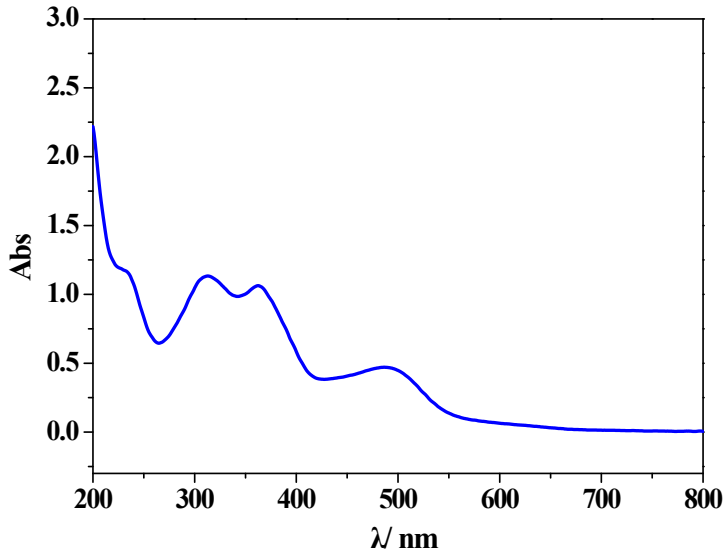

Fig. S1. The UV spectrum of complex **1** in MeCN.

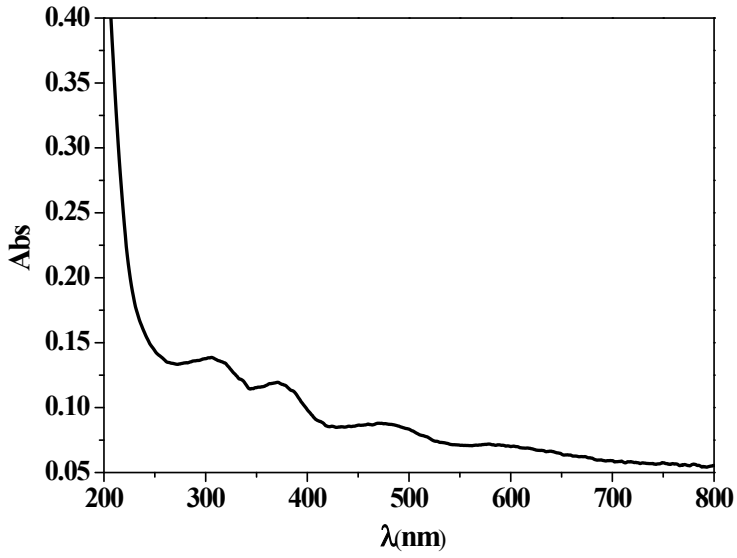

Fig. S2. The UV spectrum of complex **1** in water.

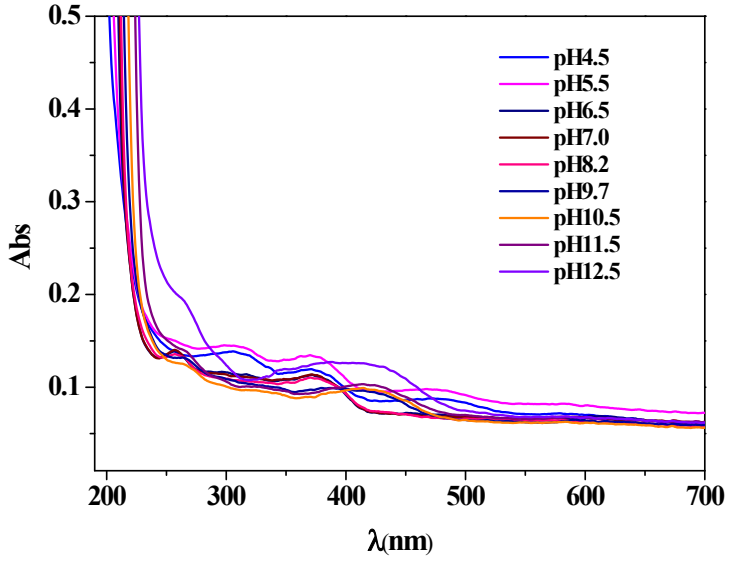

Fig. S3. The UV spectra of 0.10 mM complex **1** in 0.25 M buffered solutions in different pHs.

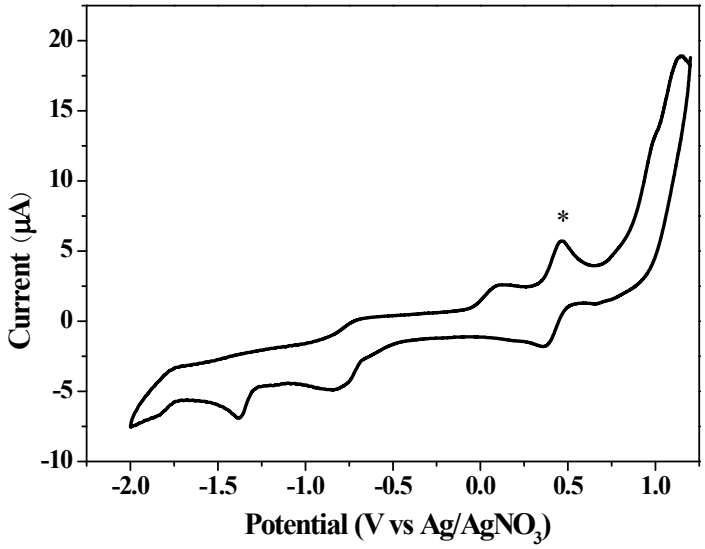

Fig. S4. Cyclic voltammogram of 3.17 mM ligand in 0.10 M of [n-Bu_4N]ClO_4 DMF solution at a glassy carbon electrode and a scan rate of 100 mV/s. (*) ferrocene internal standard.

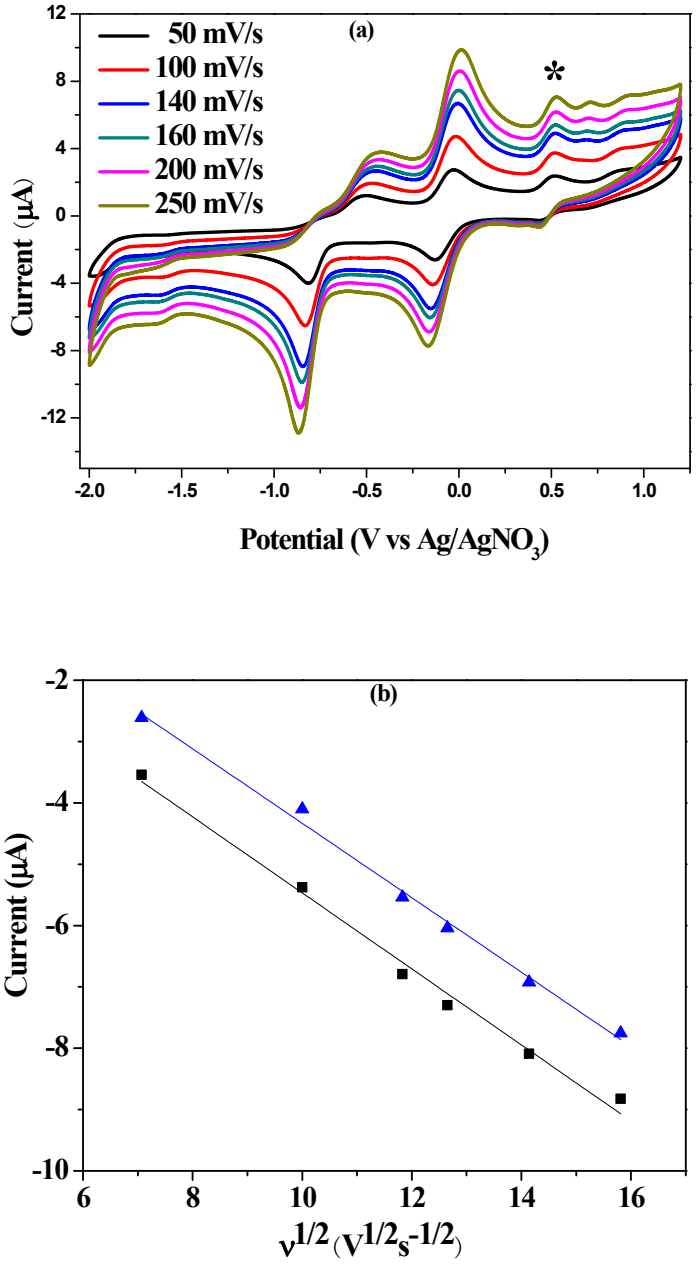

Fig. S5. (a) Scan rate dependence of precatalytic waves for a 3.17 mM solution of complex **1** in DMF, at scan rates from 50 to 250 mV/s. (b) Plot of current *vs* $\nu^{1/2}$ at -0.08 V ($Fe^{III/II}$) (blue line) and -1.55 V ($Fe^{II/I}$) (black line). Conditions: 0.10 M [n-Bu_4N]ClO_4 as supporting electrolyte, GC working electrode (1.0 mm diameter), Pt counter electrode, $Ag/AgNO_3$ reference electrode, (*) ferrocene internal standard.

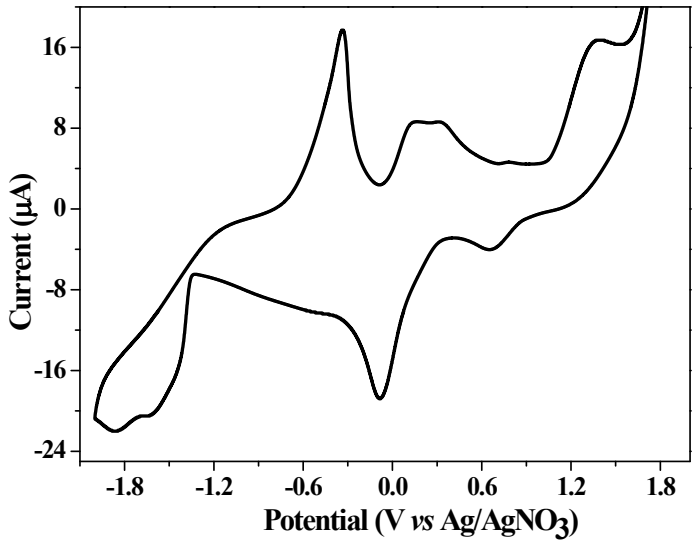

Fig. S6. CV of 3.17 mM $FeCl_3$ in 0.10 M of [n-Bu_4N]ClO_4 DMF solution. GC working electrode (1.0 mm diameter), Pt counter electrode, Ag/$AgNO_3$ reference electrode, scan rate 100 mV/s.

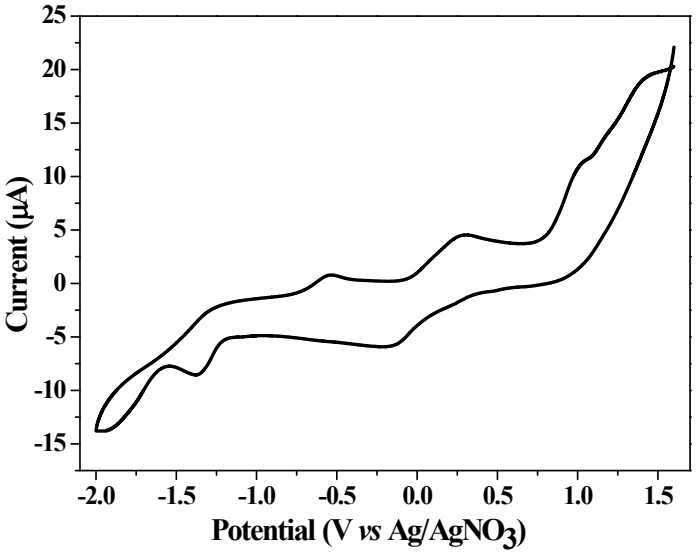

Fig. S7. CV of ligand (3.17 mM) and $FeCl_3$ (3.17 mM) (1:1) in 0.10 M of [n-Bu_4N]ClO_4 DMF solution. GC working electrode (1.0 mm diameter), Pt counter electrode, Ag/$AgNO_3$ reference electrode, scan rate 100 mV/s.

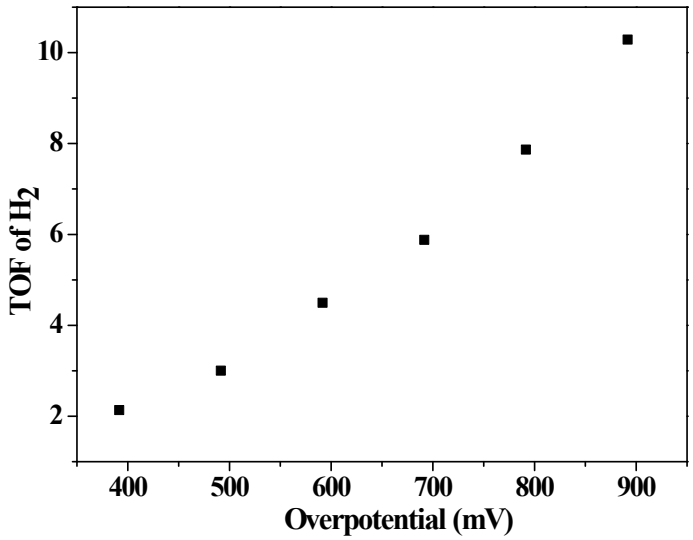

Fig. S8. Turnover frequency (mol H_2/mol catalysts/h) for electrocatalystic hydrogen production by complex **1** (5.80 μM) under overpotentials.

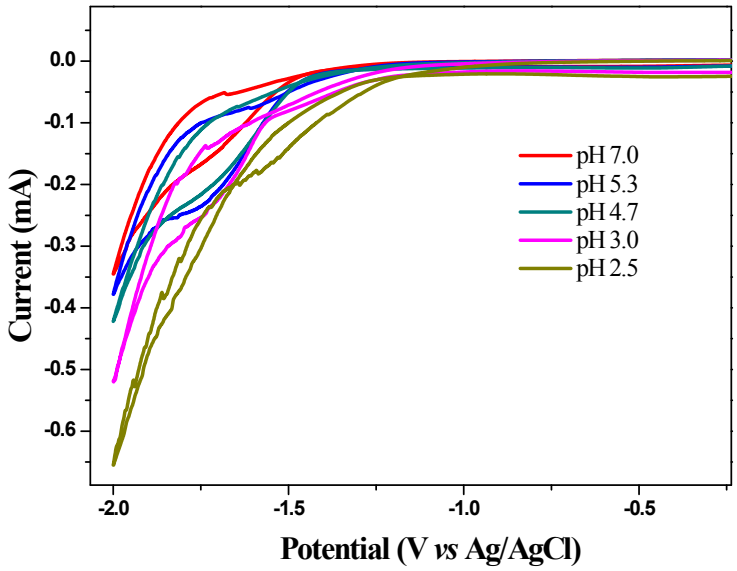

Fig. S9. Cyclic voltammograms of complex **1** (1.71 mM) in different pHs. Conditions: 0.25 M phosphate buffered solutions (KH_2PO_4 + NaOH), GC working electrode (1.0 mm diameter), Pt wire counter electrode, Ag/AgCl reference electrode.

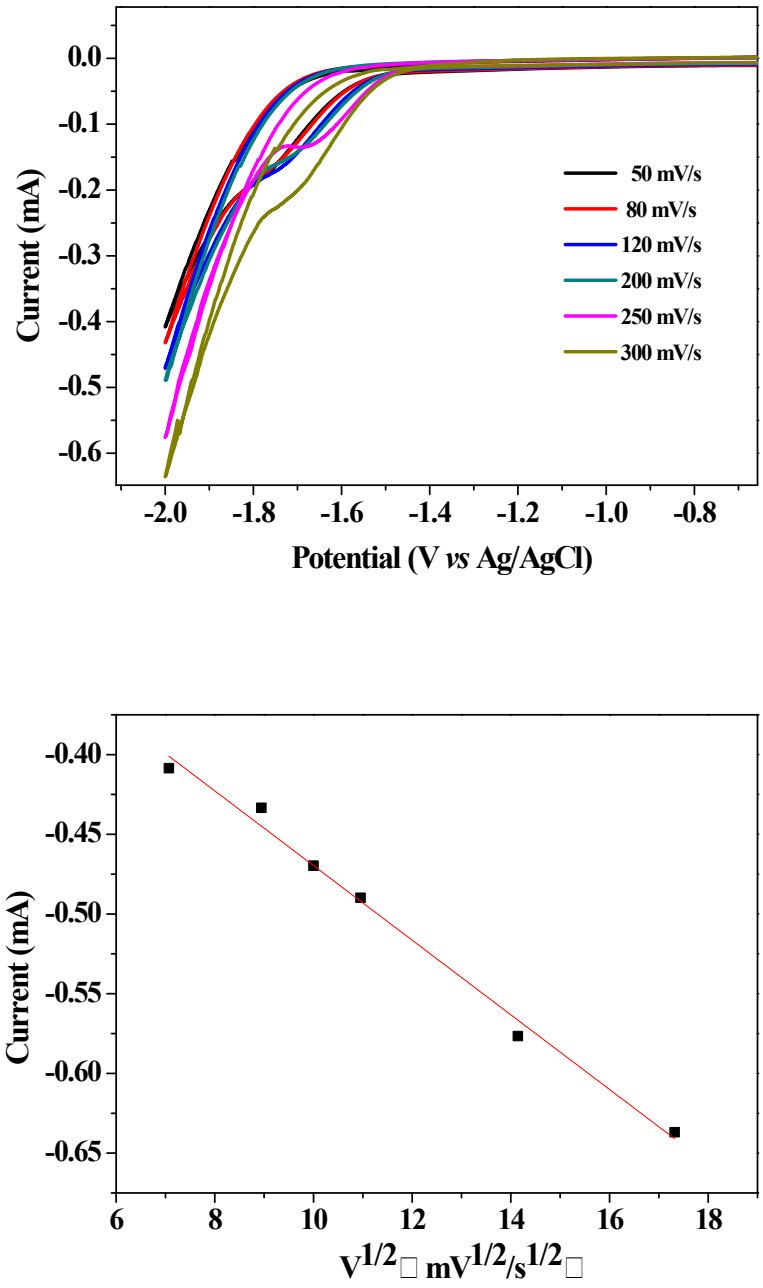

Fig. S10. Cyclic voltammogram of complex **1** (1.05 mM) in different scan rate. Conditions: 0.25 M phosphate buffered solution (pH 7.0), GC working electrode (1.0 mm diameter), Pt wire counter electrode, Ag/AgCl reference electrode.

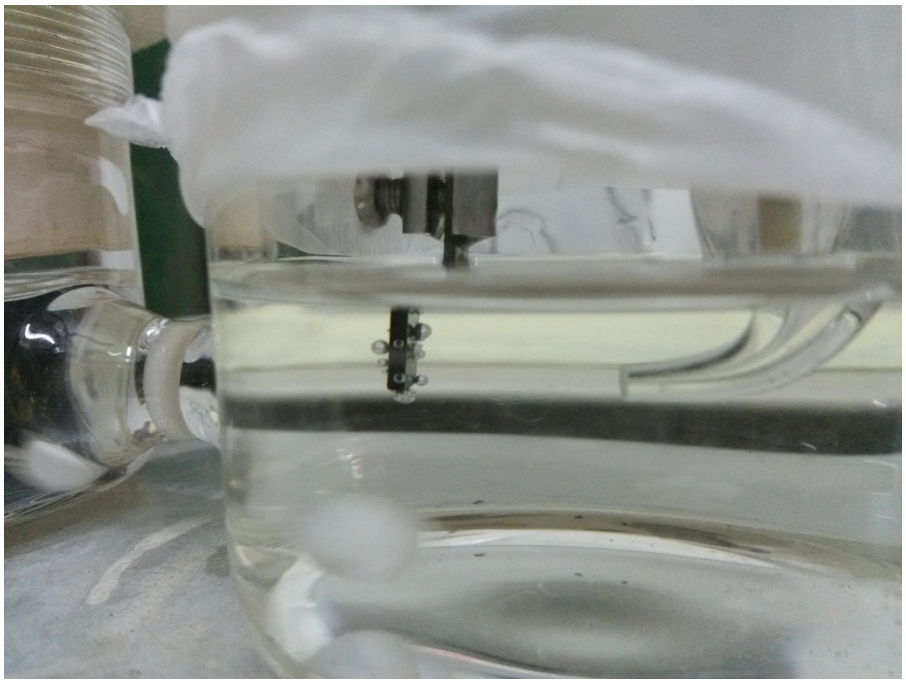

Fig. S11. Bubble forms

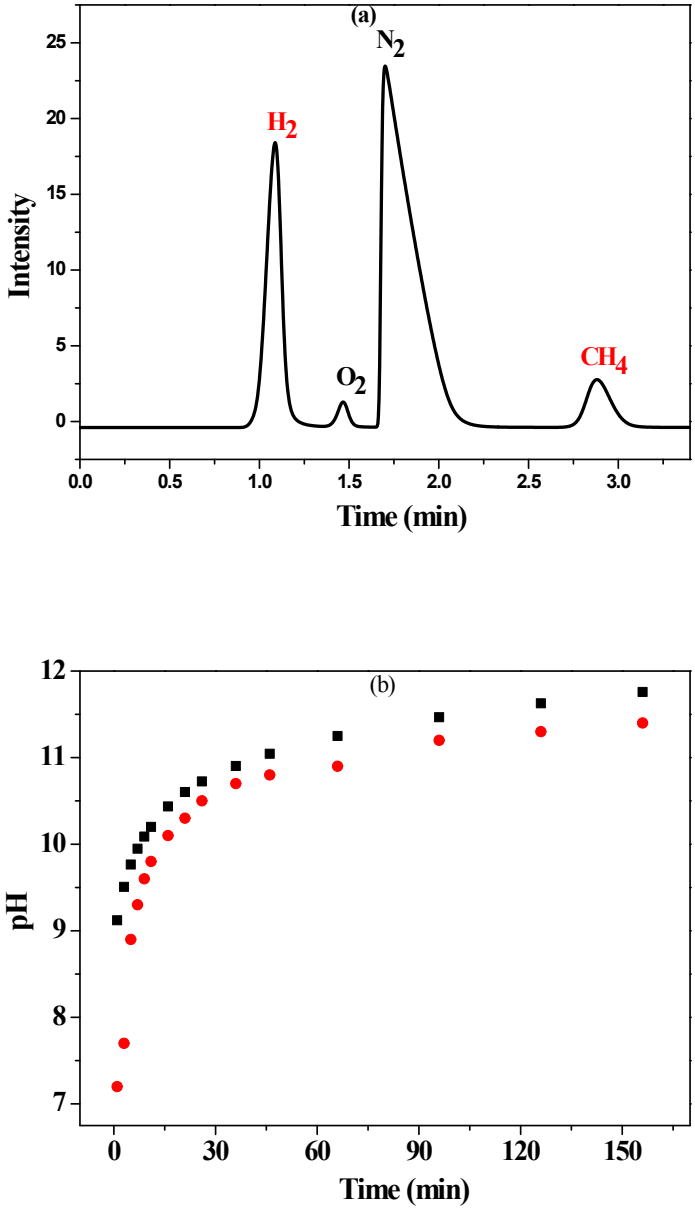

Fig. S12. (a) GC traces after a 1h controlled-potential electrolysis at −1.45 V *vs* Ag/AgCl of 17.4 μM complex **1** in 0.25 M buffer, pH 7.0. A standard of CH_4 was added for calibration purposes. (b) Measured (red) and calculated (black) pH changes assuming a 100% Faradic efficiency of complex **1** during electrolysis. (the theoretical pH change over time can be calculated by the equation of $pH = 14 + \lg \frac{\sum It}{FV}$ where I = current (A), t = time (s), F = Faraday constant (96485 C/mol), V = solution volume (0.04 L)).

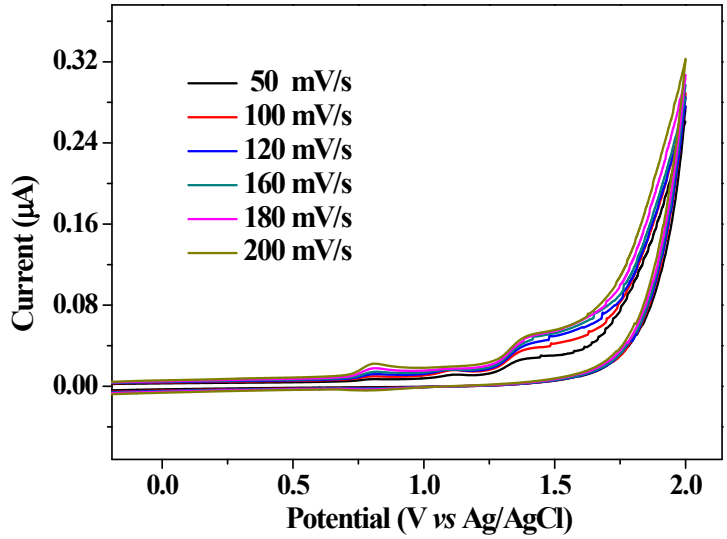
50 mV/s
100 mV/s
120 mV/s
160 mV/s
180 mV/s
200 mV/s
Current (μA)
Potential (V vs Ag/AgCl)
0.32
0.24
0.16
0.08
0.00
0.0
0.5
1.0
1.5
2.0

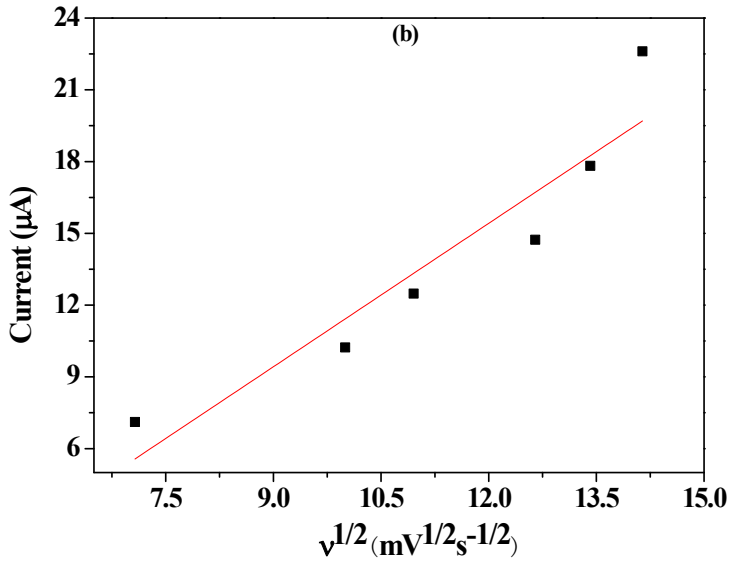
(b)
Current (μA)
ν1/2 (mV1/2s-1/2)
24
21
18
15
12
9
6
7.5
9.0
10.5
12.0
13.5
15.0

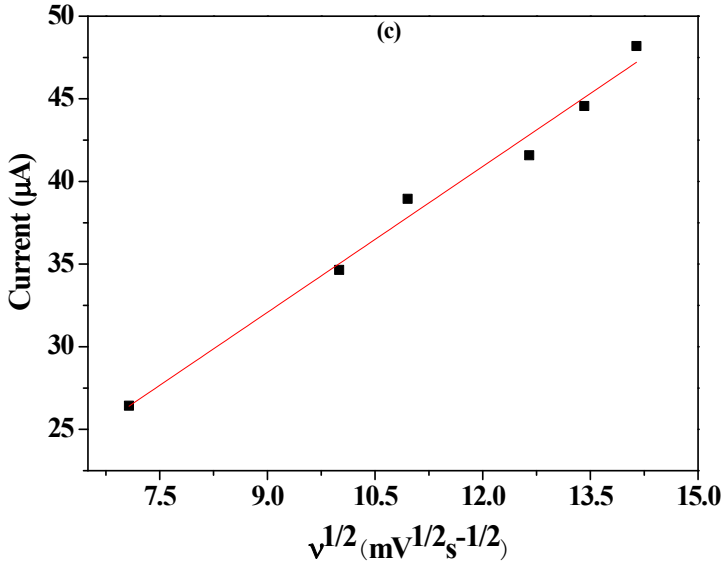

Fig. S13. (a) Scan rate dependence of precatalytic waves for $Fe^{IV/III}$ and $Fe^{V/IV}$ couples from a 1.71 mM solution of complex **1** in buffer (pH 10.5), at scan rates from 50 to 200 mV/s. (b) Linear fitting plot of i_{cat} *vs* $v^{-1/2}$ for $Fe^{IV/III}$. (c) Linear fitting plot of i_{cat} *vs* $v^{-1/2}$ for $Fe^{V/IV}$.

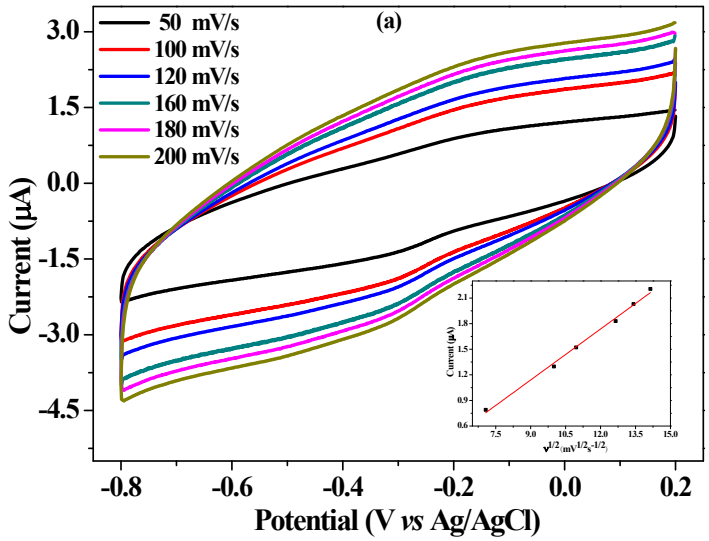

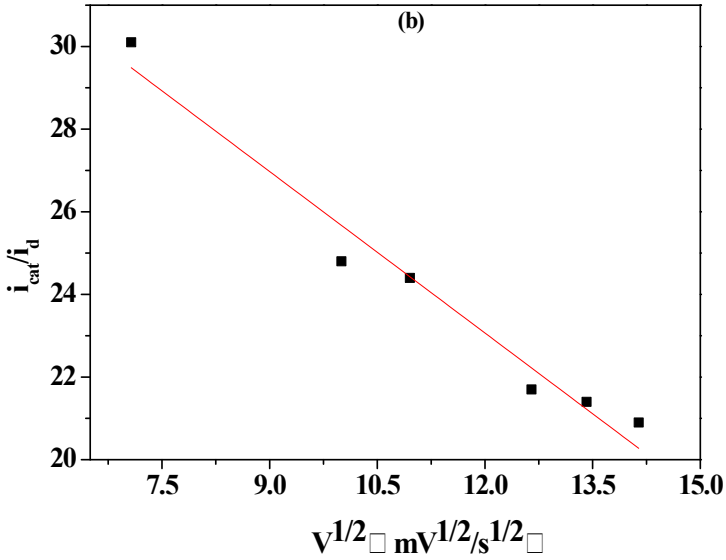

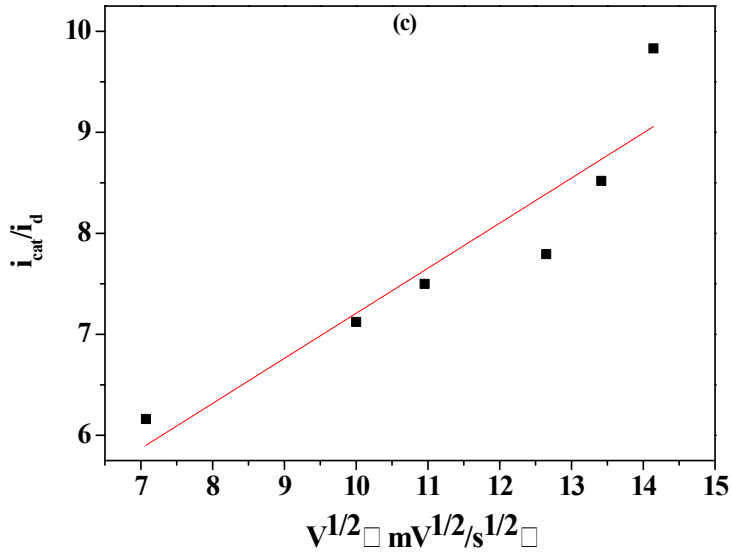

Fig. S14. (a) Scan rate dependence of precatalytic wave for a 1.71 mM solution of complex **1** in buffer (pH 10.5), at scan rates from 50 to 200 mV/s. (b) Linear fitting plot of i_{cat}/i_d *vs* $v^{-1/2}$ ($Fe^{V/IV}$) for TOF calculation. (c) Linear fitting plot of i_{cat}/i_d *vs* $v^{-1/2}$ ($Fe^{IV/III}$) for TOF calculation.

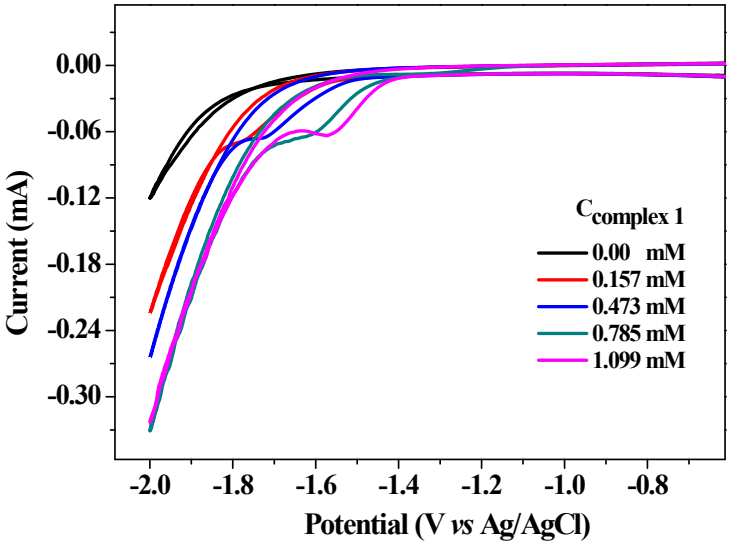

Fig. S15. Cyclic voltammograms of complex **1** in different concentrations.

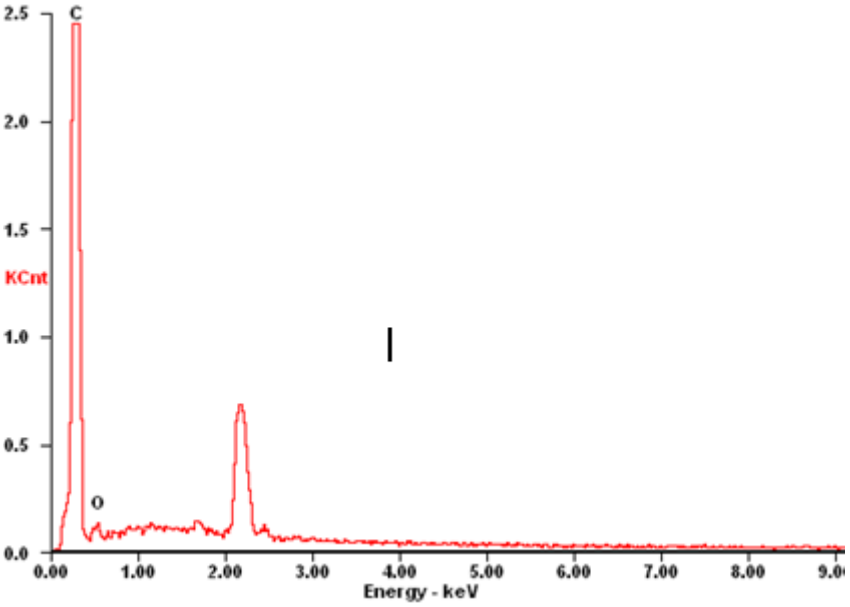

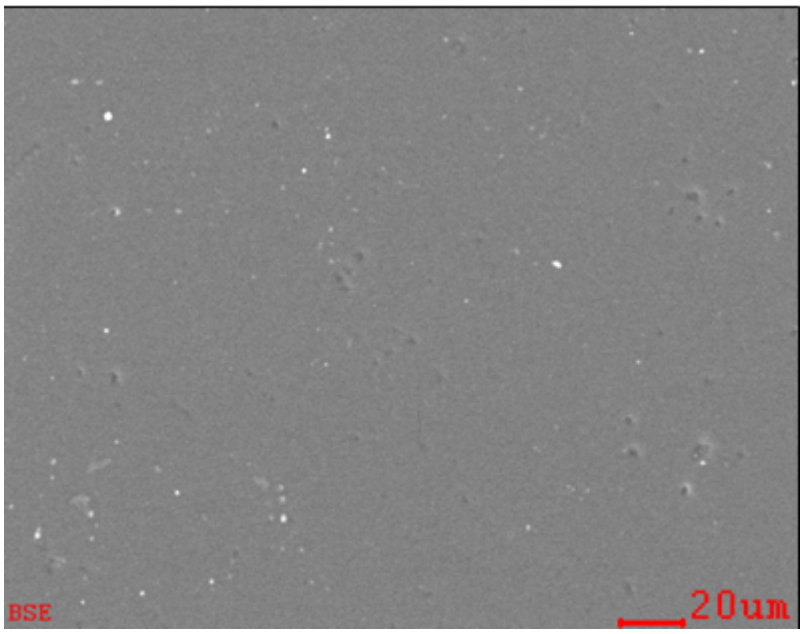

Fig. S16. ICP of a glassy carbon electrode after 4 h electrolysis. There was no significant change in the ICP after a 4 h electrolysis period.

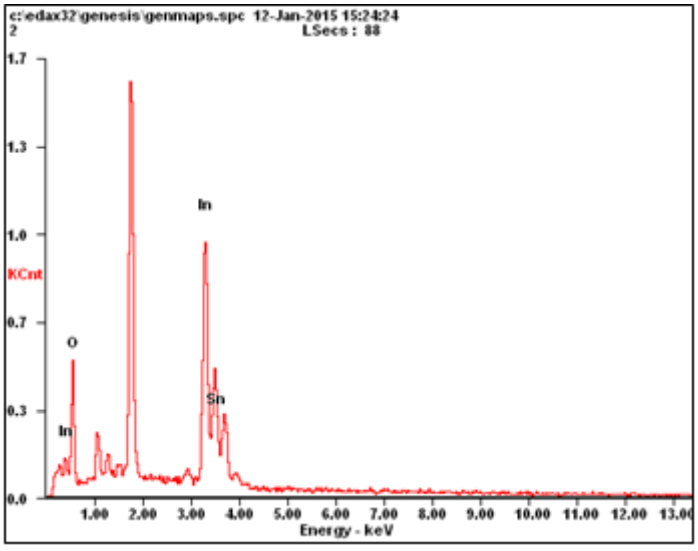

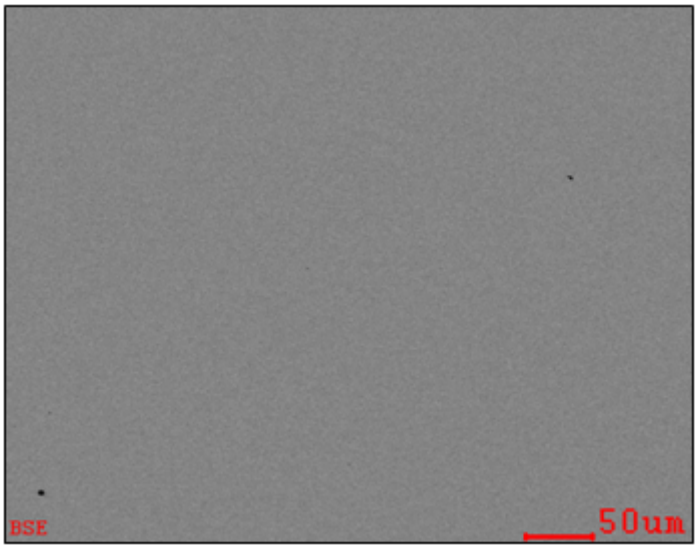

Fig. S17. ICP of an ITO electrode after 4 h electrolysis. There was no significant change in the ICP after a 4 h electrolysis period.

$$TOF = \frac{\Delta C}{F \cdot n_1 \cdot n_2 \cdot t} = \frac{0.01535C \times 3600}{96480C \cdot mol^{-1} \times 2 \times 0.232 \times 10^{-6} mol \times 120} = 10.25h^{-1}$$

Eq. S1. The calculation of TOF-1 (DMF)

$$TOF = \frac{\Delta C}{F \cdot n_1 \cdot n_2 \cdot t} = \frac{0.624C \times 3600}{96480C \cdot mol^{-1} \times 2 \times 0.12 \times 10^{-6} mol \times 120} = 808.46h^{-1}$$

Eq. S2. The calculation of TOF-2 (Buffer, pH 7.0)

$$\frac{i_c}{i_p} = 0.359 \frac{n_c}{n_p^{3/2}} \sqrt{k_{cat} / \upsilon} \qquad (2)$$

y=0.4463x-2.7450

n=4; n_p= 1

$$\frac{i_c}{i_p} = 0.359 \frac{n_c}{n_p^{3/2}} \sqrt{k_{cat} / \upsilon} = 1.413 \sqrt{k_{cat}} \times \upsilon^{-1/2}$$

$$1.413 \sqrt{k_{cat}} = 0.4463$$

$$k_{cat} = 0.01 s^{-1}$$

Eq. S3. The calculation of TOF-3

$$\frac{i_c}{i_p} = 0.359 \frac{n_c}{n_p^{3/2}} \sqrt{k_{cat} / \upsilon} \qquad (2)$$

y=--1.302x-38.697

n=4; n_p= 1

$$\frac{i_c}{i_p} = 0.359 \frac{n_c}{n_p^{3/2}} \sqrt{k_{cat} / \upsilon} = 1.413 \sqrt{k_{cat}} \times \upsilon^{-1/2}$$

$$1.413 \sqrt{k_{cat}} = -1.302$$

$$k_{cat} = 0.849 s^{-1}$$

Eq. S4. The calculation of TOF-4

Table S1 Crystal data and structure refinement for complex **1**

Crystal data	Complex **1**
Empirical formula	$C_{18}H_{12}ClFeN_4O_3$
Formula weight	423.62
Temperature/K	293(2)
λ(Å)	0.71073
Crystal system	Triclinic
Space group	P-1
a/Å	6.9901(7)
b/Å	10.9240(11)
c/Å	12.1442(13)
α/°	97.445(2)
β/°	98.875(2)
γ/°	105.900(2)
V/Å^3	866.64(15)
Z	2
Dc/Mgm^{-3}	1.623
F(000)	430
range for data collection	2.37 to 27.60deg
Reflections collected/unique	10846/3948
Goodness-of-fit on F^2	1.043
Final R indices [I>2sigma(I)]	R_1= 0.0306
	wR_2= 0.0870
R indices (all data)	R_1= 0.0395
	wR_2= 0.0922

Table S2 Selected bond lengths (Å) and angles (°) for **1**

Fe(1)-O(2)	1.8791(14)	Fe(1)-O(1)	1.9086(13)
Fe(1)-N(3)	2.1263(15)	Fe(1)-N(4)	2.1317(15)
Fe(1)-O(3)	2.2086(13)	Fe(1)-Cl(1)	2.3098(6)
O(2)-Fe(1)-O(1)	103.59(6)	O(2)-Fe(1)-N(3)	162.05(6)
O(1)-Fe(1)-N(3)	88.82(6)	O(2)-Fe(1)-N(4)	87.98(6)
O(1)-Fe(1)-N(4)	162.52(6)	N(3)-Fe(1)-N(4)	77.20(6)
O(2)-Fe(1)-O(3)	86.39(6)	O(1)-Fe(1)-O(3)	86.53(6)
N(3)-Fe(1)-O(3)	81.40(5)	N(4)-Fe(1)-O(3)	81.10(6)
O(3)-Fe(1)-Cl(1)	171.71(4)		